An Inverse Compton Process for the Excess Diffuse EUV Emission from the Virgo and Coma Galaxy Clusters

Chorng-Yuan Hwang

The excess extreme-ultraviolet (EUV) emission detected in the Virgo and Coma clusters is explained by inverse Compton scattering of cosmic microwave background photons, which are scattered by the relativistic electrons that account for the extended radio synchrotron emission of these clusters. The lower limits of the average magnetic fields of these clusters estimated from the EUV excess are close to the equipartition magnetic fields derived from radio observations, indicating that the electron energies and magnetic field energies might be close to equipartition. The excess emission suggests energy reservoirs of ~10^{61} and ~10^{60} ergs for the Coma and Virgo clusters, respectively.

The Virgo and Coma galaxy clusters have been found to emit excess EUV and soft x-ray emission compared with a hot thermal plasma model (*1*, *2*). It has been established that the x-ray emission of clusters of galaxies is thermal plasma emission from a hot intracluster gas (*3*); on the other hand, the origin of the excess EUV emission is still unknown (*4*–*6*). Excess emission due to some unknown instrumental effects has been ruled out because the excess emission was observed by the deep survey telescope (DS) of the Extreme Ultraviolet Explorer satellite (EUVE) and by the position-sensitive proportional counter of the Roentgen x-ray satellite. The interstellar medium (ISM) of our galaxy is also considered to be an unlikely explanation for the observed EUV and soft x-ray excess because the required ionization state of the ISM is very different from the actual values observed for the local and global ISM (*2*, *5*).

Lieu *et al.* (*1*, *2*) have suggested that the excess component is due to thermal emission from gases at about 5×10^5 to 1×10^6 K. An immediate consequence of such an explanation is that the gas at these temperatures would have cooled rapidly and might have accumulated cold matter with a mass of up to 10^{14} solar masses ($M_\odot$) after 10 billion years. The accumulated mass was far more than that expected from a cooling flow model, which found only 10 $M_\odot$ per year for the Virgo cluster and no evidence of mass cooling flow for the Coma cluster (*7*). Furthermore, the Hopkins Ultraviolet Telescope did not detect any significant emission of the resonance lines of O VI at wavelengths of 1032 and 1038 Å and C IV at wavelengths of 1548 and 1551 Å (the roman numerals indicate the ionization numbers) from the clusters that show excess emission (*8*); this finding is inconsistent with a gas at the inferred temperatures. Fabian (*6*) has proposed turbulent mixing layers as a viable scenario to explain the existence of a 10^6 K gas component in these clusters; however, it is hard to validate the applicability of this model because of several uncertain parameters involved in it.

Institute of Astronomy and Astrophysics, Academia Sinica, Post Office Box 1-87, Nankang, Taipei, Taiwan 115, Republic of China.

Cosmic microwave background (CMB) 3-K photons scattered by relativistic electrons can also produce EUV and soft x-ray emission (*9*). Diffuse radio emission from the Coma and Virgo clusters has been detected (*10*, *11*); the emission is synchrotron radiation emitted by the relativistic electrons in the halo regions of these clusters. The sizes of the emission halos are comparable with those of the excess EUV regions (*12*). Given the existence of the relativistic electrons, it seems likely that an inverse Compton (IC) process is operating in these clusters and scattering CMB photons to higher energy. It is possible that the excess EUV and soft x-ray radiation has an origin from the IC-scattered CMB 3-K (IC-3K) photons.

The IC-3K model can be tested by comparing the observed diffuse synchrotron radiation with the excess EUV emission. If the relativistic electrons in the Virgo and Coma clusters have a power-law energy distribution

$$N_e(E_e) = NE_e^{-p}, E_l < E_e < E_u \quad (1)$$

where N_e is the electron number density, N is a constant, E_e is the electron energy, E_l and E_u are the lower and upper cutoffs in the energy distribution, respectively, and p is the electron spectral index of a power-law distribution, the synchrotron radiation $S_S(\nu)$ emitted by these electrons is proportional to $\nu^{-(p-1)/2}$, where ν is the frequency of the radiation. The IC-3K photon flux density S_{IC}, at energy ε, scattered by the same relativistic electrons, is then given by

$$S_{IC}(\varepsilon) = (3\pi c^3 \hbar^3)^{-1}(3e/4\pi m_e c)^{-(p-3)/2} \times (kT)^{(p+5)/2} B_0^{-(p+1)/2} \frac{F(p)}{a(p)} \nu^{(p-1)/2} \times S_S(\nu)\varepsilon^{-(p+1)/2} \quad (2)$$

where e is the electron charge, c is the speed of light, $\hbar$ is the Planck's constant, m_e is the mass of an electron, k is the Boltzmann's constant, T is the temperature, B_0 is the average magnetic field in the halo regions, and $F(p)$ and $a(p)$ are the parameter functions defined by Blumenthal and Goulds (*9*, *13*).

For the Coma cluster, the relativistic electron distribution has $p = 3.68$ (*10*), and the IC photon flux density is (*14*)

$$S_{IC}(\varepsilon) = (3.41 \pm 0.61 \times 10^{-18}) \times B_0^{-2.34}\varepsilon^{-2.34} \text{ cm}^{-2} \text{ s}^{-1} \text{ keV}^{-1} \quad (3)$$

If $B_0 \approx 0.4$ μG, the IC flux within 0.1 and 0.27 keV would be about 9.87×10^{-12} ergs cm^{-2} s^{-1}. Given the ISM absorption of the Milky Way, which has a neutral hydrogen column density of $N_{HI} = 8.7 \pm 1.0 \times 10^{19}$ cm^{-2} (*2*), the absorbed flux would be about 2.9×10^{-12} ergs cm^{-2} s^{-1}, which could produce a total count rate of about 50 ± 10 count/ks in the DS. This count rate is large enough to explain the total excess count rates (45 count/ks) detected for the Coma cluster (*2*). This magnetic field is stronger by a factor of 4 than that derived from the hard x-ray observation with the Compton Gamma-Ray Observatory, which obtained a lower limit of $B_0 \approx 0.1$ μG for the Coma cluster when the IC flux density of Eq. 3 was applied to the hard x-ray data (*14*). $B_0 \approx 0.4$ μG derived from the observed excess EUV emission is close to the equipartition magnetic fields and the large-scale magnetic fields for the Coma cluster obtained independently from several different observations (*15*–*19*), which indicates that the IC-3K model is consistent with these observations and that the electron energy and magnetic energy might be close to equipartition.

The thermal flux of the Coma cluster was determined from the emission of a hot gas estimated from the Mewe-Kaastra (MEKA) thermal plasma code (*20*) with the model parameters of (*2*), and the IC-3K flux was derived from the radio halo emission with $B_0 = 0.4$ μG. The estimated thermal flux dominates at energy around 1 keV (Fig. 1); the contribution of the IC-3K flux become significant only at lower energy, around 0.1 to 0.2 keV (Fig. 1). The excess emission is prominent in the DS because the DS detector has the highest response around 0.15 keV. The IC-3K flux was ignored in earlier x-ray observations because it did not contribute significantly to the total flux in the energy ranges of these observations.

The IC-3K EUV emission is produced by the relativistic electrons with energies that are unobservable from ground-based radio telescopes. The radio frequencies observed for the halo of the Coma cluster range from 10 to 1400 MHz, which correspond to Lorentz energy factors, γ, from 2500 to 30,000 (*21*), if $B_0 = 0.4$ μG. On the other hand, the IC-3K EUV photons detected by the DS are primarily scattered by the electrons of $\gamma \approx 410$. It might be questioned whether the electron spectrum can be extrapolated to low energy. It has been suggested that the electron distribution between $\gamma = 100$ and 1000 might be flatter than the extrapolated power law observed at higher energies (*22*). Particularly, if the steepness of the electron spectrum is caused by dominant energy losses of synchrotron radiation and IC scattering, which have energy loss time scales inversely proportional to electron energies, the low-energy electrons might be flatter because the time scales of energy loss are longer for the low-energy electrons. However, the half-life of electrons with $\gamma = 410$ is about 2.7×10^9 years (*21*). This result implies that the electrons at this low-energy region are also affected by the same energy loss mechanism and aging cannot cause significant flattening at this low energy. Other situations that might lead to spectrum flattening at low energies, for example, a strong magnetic field or a high electron density (*22*), are not applicable to the Coma cluster because of its weak magnetic field and low electron density.

Nonetheless, it is important to examine whether any potential flattening of the unobservable electron distribution might limit the applicability of the IC-3K model for the EUV excess. If the electron distribution begins to flatten at $\gamma = 1000$, then the IC-3K model can still account for half of the observed EUV excess even if the electron spectral index is flattened to $p = 3.0$, and it can account for one-third of the observed excess if $p = 2.7$ (Fig. 2). If $B_0 \sim 0.2$ μG, as has been suggested by some observations (*15*, *17*, *19*), the IC-3K process can explain the observed EUV excess even if $p = 2.2$. Because the flattening of the electron spectral index Δp is unlikely to be more than 1 (*23*), I find that the IC-3K process always contributes some excess EUV photons given $p = 2.6$ to 3.6 and $B_0 = 0.2$ to 0.4 μG (Fig. 2). The reservoirs of the energy and the relativistic electrons are about $\sim 10^{61}$ and $\sim 10^{65}$ ergs, respectively, for $p = 3.68$ and are smaller if the electron spectrum flattens at low energy. The predicted gamma-ray radiation due to the IC scattering of the thermal x-ray and optical radiation of the Coma cluster from these low-energy electrons is below the detection limits of current gamma-ray observations.

For the Virgo cluster, the halo emission is dominated by an asymmetric structure within a 12 arc min by 16 arc min region (*11*). This dominant halo is roughly within the 7–arc min radius of the cluster; the radio emission outside the 7–arc min radius is less clear (*11*). Here, I compare the IC-3K EUV and radio synchrotron emission only within the central 7–arc min radius of the Virgo cluster. The IC-3K photon flux density within the radio halo is

$$S_{IC}(\varepsilon) = (1.9 \times 10^{-15}) \times B_0^{-2.17} \varepsilon^{-2.17} \text{ cm}^{-2} \text{ s}^{-1} \text{ keV}^{-1} \quad (4)$$

The count rate in the DS caused by this IC-3K flux could explain the excess emission (*1*) if $B_0 \approx 1.25$ μG; the reservoirs of the energy and the relativistic electrons are about $\sim 10^{60}$ and $\sim 10^{63}$ ergs, respectively. The B_0 derived for the Virgo cluster is much higher than that for the Coma cluster; however, the equipartition magnetic fields derived from radio observations (*11*, *24*, *25*) of the Virgo cluster are also higher and are close to the B_0 derived from the EUV excess, which again indicates the consistency between the magnetic field derived from the IC-3K EUV model and those derived from other observations.

Therefore, IC scattering of the CMB 3K photons is a feasible model to produce the excess EUV photons of clusters of galaxies detected by EUVE, such as the Coma and Virgo clusters. This process is the most natural and physically grounded mechanism to account for the excess EUV emission for the Coma and Virgo clusters because of the existence of relativistic electrons in these clusters. The lower limits of the B_0 values derived from the EUV excess are higher than previous values obtained from hard x-ray observations and close to the equipartition magnetic fields. Furthermore, the synchrotron radiation emitted from the relativistic electrons and the observed excess EUV emission are quantitatively consistent with each other in the IC-scattering scheme. Although the existence of a 10^6 K gas component in these clusters cannot be excluded, there is no need for the existence of such a warm gas to explain the excess EUV emission for these two clusters; at least, the amount of the warm gas required should be reduced.

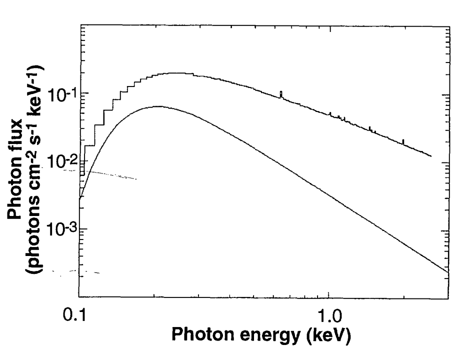

Fig. 1. The IC-scattered CMB photon flux and the thermal emission from the hot gas component of the Coma cluster. The thermal emission of the hot component (histogram) was estimated from the MEKA plasma code with parameters within the inner 15–arc min radius of the cluster (2). The IC-3K photon flux (solid line) was calculated from Eq. 3 with $B_0 = 0.4$ μG. The hot component has a temperature $kT = 8.21$ keV and a metal abundance $A = 0.21$. The ISM absorption of $N_{HI} = 8.7 \times 10^{19}$ was taken into account for both fluxes.

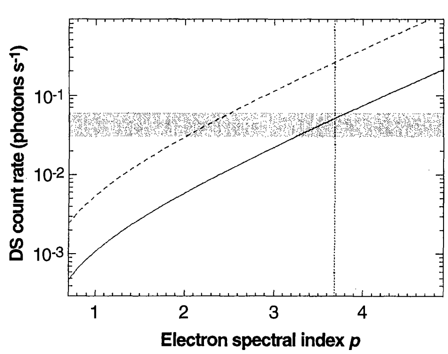

Fig. 2. The expected count rates in the DS for the Coma cluster at different electron spectral indices. The break point of the electron spectrum was assumed to be at $\gamma = 1000$. The expected count rates with $B_0 = 0.4$ μG (solid line) and $B_0 = 0.2$ μG (dashed line) were calculated from Eq. 3 folded with the ISM absorption ($N_{HI} = 8.7 \times 10^{19}$) and the effective area of the DS. The observed excess EUVE DS count rate and its uncertainty are indicated by the gray area. The vertical dotted line indicates the observed spectral index $p = 3.68$.

REFERENCES AND NOTES

1. R. Lieu *et al.*, *Astrophys. J.* **458**, L5 (1996).
2. R. Lieu *et al.*, *Science* **274**, 1335 (1996).
3. C. Sarazin, *Rev. Mod. Phys.* **58**, 1 (1986).
4. A. C. Fabian, *Science* **271**, 1244 (1996).
5. S. Bowyer, M. Lampton, R. Lieu, *ibid.* **274**, 1338 (1996).
6. A. C. Fabian, *ibid.* **275**, 48 (1997).
7. ———, *Annu. Rev. Astron. Astrophys.* **32**, 277 (1994).
8. W. V. D. Dixon, M. Hurwitz, H. Ferguson, *Astrophys. J.* **469**, L77 (1996).
9. G. R. Blumenthal and R. J. Gould, *Rev. Mod. Phys.* **42**, 237 (1970).
10. K.-T. Kim, P. P. Kronberg, P. E. Dewdney, T. L. Landecker, *Astrophys. J.* **355**, 29 (1990).
11. H. Andernach, J. R. Baker, A. von Kap-herr, R. Wielebinski, *Astron. Astrophys.* **74**, 93 (1979).
12. R. Hanisch and W. Erickson, *Astron. J.* **85**, 183 (1980).
13. The definitions for $F(p)$ and $a(p)$ are

$$F(p) = 2^{p+3}\left[\frac{(p^2+4p+11)}{(p+3)^2(p+1)(p+5)}\right] \times \Gamma[(p+5)/2]\zeta[(p+5)/2]$$

and

$$a(p) = \frac{2^{(p-1)/2}\sqrt{3}\Gamma[3p-1)/12]\Gamma[3p+19)/12]\Gamma[(p+5)/4]}{8\pi^{1/2}(p+1)\Gamma[(p+7)/4]}$$

where Γ and ζ are the Riemann Γ function and the ζ function, respectively.
14. Y. Rephaeli, M. Ulmer, D. Gruber, *Astrophys. J.* **429**, 554 (1994).
15. R. J. Hanisch, *Astron. J.* **85**, 1565 (1980).
16. ———, R. G. Strom, W. J. Jaffe, *Astron. Astrophys.* **153**, 9 (1985).
17. K.-T. Kim, P. P. Kronberg, G. Giovannini, T. Venturi, *Nature* **341**, 720 (1989).
18. G. Giovannini, L. Feretti, T. Venturi, K.-T. Kim, P. P. Kronberg, *Astrophys. J.* **406**, 399 (1993).
19. L. Feretti, D. Dallacasa, G. Giovannini, A. Tagliani, *Astron. Astrophys.* **302**, 680 (1995).
20. R. Mewe, E. H. B. M. Gronenschild, G. H. J. van den Oord, *Astron. Astrophys. Suppl. Ser.* **62**, 197 (1985).
21. D. E. Harris and J. E. Grindlay, *Mon. Not. R. Astron. Soc.* **188**, 25 (1979).
22. D. E. Harris, in *Low Frequency Astrophysics from Space*, N. E. Kassim and K. W. Weiler, Eds. (Lecture Notes in Physics no. 362, Springer-Verlag, Berlin, 1990), pp. 252–261.
23. V. S. Ptuskin, in *Astrophysics of Cosmic Rays*, V. L. Ginzburg, Ed. (Elsevier, Amsterdam, 1990), pp. 171–215.
24. B. Dennison, *Astrophys. J.* **236**, 761 (1980).
25. J. P. Vallee, *Astron. J.* **99**, 459 (1990).
26. I thank D. E. Harris, S. Bowyer, R. Lieu, L.-W. Chen, and K. Y. Lo for useful discussions and comments. I also acknowledge support from Academia Sinica and the National Science Council of the Republic of China in Taiwan.

8 July 1997; accepted 30 October 1997

A Pulsar, the Heliosphere, and Pioneer 10: Probable Mimicking of a Planet of PSR B1257+12 by Solar Rotation

Klaus Scherer,*† Horst Fichtner, John D. Anderson, Eunice L. Lau

Doppler data generated with the Pioneer 10 spacecraft's radio carrier wave between 1987 and 1995 show a 25.3-day periodicity which is related to the solar rotation. The timing data of the pulsar PSR B1257+12 also show a periodicity of 25.34 days, which has been explained as a signature of the pulsar's barycentric motion in response to the existence of a small moon-like object. However, because PSR B1257+12 is located close to the ecliptic and because the timing variations are in the range of microseconds, it is likely that the pulsar signal is affected by the same mechanism acting on the Pioneer 10 Doppler data. Hence, the hypothesized inner planet around PSR B1257+12 is probably an artifact of the heliosphere.

Variations in the timing data of the pulsar PSR B1257+12 with periodicities of 25.34, 66.54, and 98.22 days have been explained by its motion around the barycenter, defined by the pulsar and three hypothesized planets (*1*). In fitting these data, multibody simulations were used to describe the planetary evolution over tens of years (*2*), and, with a vectorial integration method (*3*), it has been shown that the three-planet system would be stable over some hundreds of thousands of years.

Despite this plausible explanation of the timing data, the three-planet hypothesis has to be checked against other interpretations. In particular, as has been demonstrated (*4*) in connection with the suspected extrasolar planet around 51 Pegasi, serious consideration has to be given to the question of whether the planets are real. In light of this, we demonstrate that the innermost moon-like planet around PSR B1257+12 probably does not exist.

We base this hypothesis on the dominant period in the Pioneer 10 (P10) radio Doppler data (*5*) of 25.3 days, which is indistinguishable from the suspected revolution period of the inner planet around PSR B1257+12. The P10 Doppler data are obtained by a "two-way radio link" experiment, where a signal with a frequency $f = 2.1$ GHz is transmitted from Earth (uplink), transponded by the spacecraft, and hours later is received back at Earth (downlink). With a local oscillator (a highly stable hydrogen maser), it is possible to determine the Doppler shift to an accuracy of better than 1 mHz (*6*). After removing systematic changes in the position and velocity of P10 caused by the motion of the planets and the moon, periods of 13.3 days (*7*), 25.3 days (Fig. 1), and about 1 year (Fig. 2) (*8*) remained. The periods cannot be produced as a result of an acceleration of the spacecraft by the ram pressure of the solar wind ($a_{ram} \approx 5 \times 10^{-17}$ km s^{-2}) or by the solar radiation pressure ($a_{rad} \approx 5 \times 10^{-15}$ km s^{-2}), because their contribution is orders of magnitude smaller than the standard error in the reduced Doppler data.

To test the idea that the solar wind patterns are responsible for these P10 periodicities, we calculated the autocorrelation of the reduced Doppler data (Figs. 2 and 3) and compared it with the cross-correlation of the Doppler data with the solar wind proton density recorded by P10, by Voyager 2 (V2) (Fig. 2), and by the Interplanetary Monitoring Platform (IMP) (*9*) spacecraft (Fig. 3). The cross-correlation functions have a shape similar to that of the autocorrelation function (Fig. 2). The relative shift between the two cross-correlation functions can be explained by the different heliocentric distances (r) and ecliptic latitudes (β) and longitudes (λ) of P10 and V2. Although the cross-correlation is performed using the observed proton density data, the result is valid for the unobserved electron density too, because of the quasi-neutrality of the solar wind. In addition to the P10 and V2 plasma data, we correlated the reduced Doppler data with the plasma data obtained by the IMP spacecraft at 1 astronomical unit (AU) (Fig. 3). In this case, the auto- and cross-correlation functions have different shapes for larger time lags, but are very similar to each other for short time lags.

To determine any periodicities shorter than 1 year, we applied the maximum entropy method to a 9-month (*10*) coherent raw Doppler data set (Fig. 1) in 1993. The data show two periods of 25.3 and 13.3 days at a confidence level >95% and periods of 52.9, 18.5, and 11.2 days at a confidence level >50%. Here, we are interested only in the 25.3-day period, which can be explained as follows: In the ecliptic plane, the radio wave propagates through the interplanetary medium, which is not uniform but resembles the rotation of the sun, especially the structured patterns induced by the sector struc-

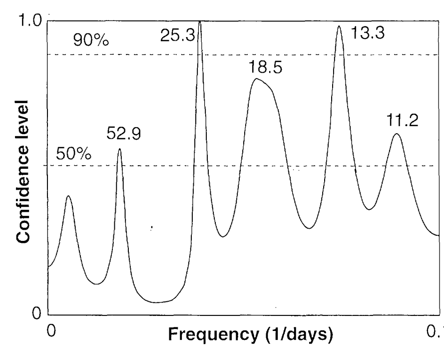

Fig. 1. Periodogram calculated by the maximum entropy (all poles) method for reduced P10 Doppler data over an interval of about 9 months centered on solar opposition.

K. Scherer, J. D. Anderson, E. L. Lau, Jet Propulsion Laboratory, Mail Stop 301/230, Pasadena, CA 91119, USA.
H. Fichtner, Institut für Astrophysik und Extraterrestrische Forschung der Universität Bonn, Auf dem Hügel 71, D-53121 Bonn, Germany.

*To whom correspondence should be addressed. E-mail: scherer@lindust.mpae.gwdg.de
†Present address: Max-Planck-Institut für Aeronomie, D-37191 Katlenburg-Lindau, Germany.